IEEE Transactions on Aerospace and Electronic Systems, Volume 59, Issue 2, April 2023, pp. 1067-1083
DOI:10.1109/TAES.2022.3197103

Online Trajectory Replan for Gliding Vehicle Considering Terminal Velocity Constraint

Youngil Kim, Namhoon Cho, Jongho Park, Youdan Kim, *Senior Member, IEEE*

Abstract

Controlling the terminal velocity can improve the effectiveness of guided missiles. In particular, a ballistic missile propelled by solid rocket motors can successfully accomplish its mission when it hits the target at an appropriate speed. In this study, a method for modifying the trajectory of gliding vehicle, i.e., gliding ballistic missiles is proposed to meet the terminal velocity constraint by reflecting the effects of the environment during a flight. The proposed framework consisting of trajectory generation and dynamic propagation compensates for errors due to uncertainties in real time. The trajectory generation step provides various trajectories that satisfy the given constraints based on information about the current state. The dynamic propagation step efficiently predicts the terminal velocity for each of the generated trajectories and finds the trajectory with the lowest terminal speed error. A numerical simulation is performed considering various conditions to demonstrate the performance of the proposed method.

Index Terms

Terminal Velocity Constraint, Trajectory Generation, Dynamic Propagation

I. Introduction

Recently, ballistic missiles are required to perform more complicated tasks in an uncertain environment over a wide range of flight altitudes. And, tactical missiles are undertaking a mission to destroy a concealed target in complex terrain. At the same time, the survivability of the missiles have been threatened due to the improvement of the air defense system.

It is very important for missiles to impact a target with an appropriate speed. A faster-than-expected terminal speed leads not only to reduced viability of the warhead but also to excessive amount of penetration, resulting in minor collateral damage. On the other hand, if the terminal speed is too low, it is difficult to approach the target because the possibility of being neutralized increases. Therefore, the capability to meet the required terminal speed through planning and control is crucial for attack effectiveness.

This research has been supported by the Institute of Advanced Aerospace Technology, SNU.

Y. Kim, and Y. Kim are with the Institute of Advanced Aerospace Technology, Department of Aerospace Engineering, Seoul National University, Seoul 08826, Republic of Korea (email: calav3@snu.ac.kr; ydkim@snu.ac.kr).

N. Cho is with the Centre for Autonomous and Cyber-Physical Systems, School of Aerospace, Transport and Manufacturing, Cranfield University, Cranfield, Bedfordshire, MK43 0AL, United Kingdom (email: nhcho91@gmail.com).

J. Park is with the Department of Military Digital Convergence, Department of AI Convergence Network, Ajou University, Suwon 16499, Republic of Korea (email: parkjo05@ajou.ac.kr).

However, achieving the appropriate terminal speed of the ballistic missile is a challenging problem. First, a Solid Rocket Motor (SRM) generates different forces depending on temperature, pressure, and imperfections during the manufacturing process. Because of the irregular nature of a thrust profile, the actual position and velocity after burnout show discrepancy from predicted values. The thrust variance manifests itself as a large dispersion in the initial energy of the missile for the glide phase. Second, various environmental uncertainties should be considered in flight planning to provide a wide operating range. It is difficult to fully reflect the influence of environment prior to launch because the atmospheric conditions including the wind cannot be accurately predicted. Third, the maneuver is mainly confined to the vertical plane because a ballistic missile aims to reach the target as quickly as possible. The horizontal maneuver is limited only to minor heading error correction, leaving the planner with not enough degree-of-freedom for energy management. Fourth, prediction of the terminal velocity is difficult to be done analytically due to the dependence on the missile dynamics. Terminal velocity is determined by the maneuver taken by the vehicle as well as the environment [1].

Research on terminal velocity control has been conducted for launch vehicles, but in a different context concerning orbit insertion accuracy. Perkins [2] studied a linear-tangent steering program for controlling nozzles to reach the target. After that, various optimization methods have been proposed to modify the trajectory considering the energy. Several iterative methods for velocity vector control to reach the target orbit were developed in [3]–[6]. Williamson et al. [7] proposed the perturbation method to generate the optimized shuttle trajectory. Studies on energy management were also conducted under assumptions such as neglecting the aerodynamic force and parametrizing the geometric shape of the trajectory. Zarchan [8] developed the general energy management system. White proposed the iterative method with Lambert's guidance [9] and cutoff time control considering the flight time [10]. Kim and Um [11] suggested a method to control the flight path angle of a vehicle in the boost phase. Wang et al. [12] proposed the spline-line based energy management guidance for ascending solid rocket vehicles. Ascent trajectory design concept was developed to increase flight performance of launch vehicle [13]. Terminal speed control has also been studied for re-entry vehicles, however, the methods developed are not suitable for ballistic missiles. A re-entry vehicle should fly with a velocity within a specific range to enter the atmosphere. Dong and Sushnigdha [14], [15] designed an optimal trajectory that generated a bank angle considering the constraints within the terminal velocity. Kraemer and Ehlers [16] showed that the energy could be regulated by creating a trajectory shape or controlling the velocity with a specific actuator used in the re-entry vehicle. Studies have also been conducted to control the energy by adjusting the angle of the vehicle to change its trajectory shape [17], [18]. Re-entry vehicle maneuvers in the horizontal plane or uses actuators such as speed brakes or parachutes to control the velocity. However, it is inappropriate for ballistic missiles to perform lateral maneuvers, which increase the length of the trajectory on the horizontal plane, because it is important to hit the target as quickly as possible. Additionally, installing additional actuators on the missile is inappropriate due to the bad flight characteristics at high-velocity regions resulting from the aerodynamic characteristics caused by the structural shape of the vehicle.

On the other hand, guidance methods considering the energy management requirements have been studied for missiles, while majority of them are focused on offline planning and computationally heavy. The approach to design the energy-dissipating trajectories with certain path primitives is a solution to control the energy of ballistic

missiles [19]–[23]. The Pythagorean-Hodograph (PH) curve, which is useful for adjusting the arc length, was adopted on the horizontal plane to satisfy the required terminal velocity [24]. A deep learning-based real-time method for a hypersonic vehicle was proposed to reach a fixed target considering energy consumption [25]. Vector field-based method was used to generate the trajectory for satisfying the specific constraints [26], [27]. Lee et al. [28] suggested the vector filed-based guidance law for gliding air-to-ground vehicle. The guidance law was designed to control the speed and impact angle control of gliding vehicle. By converting the guidance problem into a reinforcement learning problem, neural networks were trained within the available energy consumption to generate optimal trajectories and guidance command. Li et al. [29] proposed a deep reinforcement learning-based guidance law for trajectory generation considering uncertain environments. Another approach is to utilize predictive methods. The terminal velocity of the vehicle can be estimated by the trajectory shape [8], [30]–[35]. Kim et al. [1] proposed a method to determine an appropriate waypoint by predicting energy reduction according to the path of missile assuming that the environmental model was known in advance.

Note that an efficient planning algorithm enough to enable online replanning is required because the actual trajectory deviates from the one predicted offline due to the model uncertainties. There exist multiple trajectories satisfying the terminal velocity constraint while having the same initial and terminal conditions. Therefore, online modification is necessary (i) to find various trajectories satisfying the terminal velocity constraint, (ii) to efficiently predict the terminal velocity for each trajectory, and (iii) to find the most appropriate trajectory in real time.

To address the difficulties described above, an online trajectory planning method for ballistic missiles is proposed to meet the terminal velocity constraint. The proposed method generates multiple trajectories and quickly estimates the terminal velocity of each trajectory so that the one with the minimum velocity error can be chosen as the solution. The proposed framework is divided into (i) a trajectory generation algorithm that finds a path satisfying geometric constraints and (ii) a dynamic propagation algorithm that predicts the terminal velocity for a given path. In the trajectory generation algorithm, the altitude is defined as a polynomial of the downrange, and the problem is formulated as a Quadratic Program (QP) using a specific objective function to obtain the optimal solution. The dynamic propagation algorithm employs numerical integration to solve the differential equation describing the change in speed along the given path. Assuming that the vehicle perfectly generates the normal acceleration needed to realize the given path, the speed dynamics with respect to the downrange becomes a scalar relation, which enables efficient speed prediction.

The main contribution of this study is that the proposed method can generate a flight trajectory of a ballistic missile satisfying the terminal velocity constraint in real time. The proposed method is capable of quick trajectory generation while reflecting the mission requirements to have the desired form of trajectory. The combination of convex optimization for generating feasible path candidates and scalar dynamics integration for speed prediction is the key enabler for efficient planning. The proposed method overcomes the shortcomings of the existing methods developed for velocity control that are not suitable for ballistic missiles. Moreover, the trajectory generation strategy can be useful in the missile development process.

This paper is organized as follows. In Sec. II, the problem statement considered in this study is addressed. Kinematic models and dynamic models are described, and the problem with the proposed framework is explained.

In Sec. III, the trajectory generation algorithm and dynamic propagation algorithm are proposed. The proposed framework generates various trajectories and calculates the terminal velocity errors. The results of numerical simulations are shown and analyzed in Sec. IV. Finally, conclusion is given in Sec. V.

II. Problem Statement

A. Mission Characteristics

The trajectory of ballistic missiles considered in this study has the following characteristics. First, the missile motion is confined mostly to the vertical plane because the missile should hit the target as quickly as possible. Usually, the missile does not perform a horizontal maneuver unless certain constraints exist for a specific mission or the problem of the survivability of the missile. Additionally, maneuvering only on the vertical plane conserves the energy of the missile. It directly contributes to an increase in the operational range and a decrease in the consumption of propellant. Second, the missile, which should satisfy the terminal velocity constraint, generally flies along the curved trajectory in the low-altitude areas, where the air density is high enough to effectively perform maneuvers through aerodynamic control. In high-altitude areas, the energy dissipation effect is insignificant due to the low density of air. Accordingly, the missile should dissipate its energy at low altitudes. Because of the conditions imposed on the maneuver plane and the altitude, ballistic missiles prefer to alternate between ascending and descending maneuvers.

B. Model Equations

Velocity control systems such as air brakes or parachutes are not suitable for ballistic missiles flying in aerodynamic regions at supersonic speeds. For this reason, only aerodynamic control surfaces are considered in this study as actuators. Note that controlling the missile velocity is difficult when the missile flies in high-altitude areas, i.e., in low-air-density areas. In this study, the objective of the system is to satisfy the terminal velocity constraint while the missile flies in the low-altitude region. Therefore, dynamic models of the missile in the high-air-density region are required. Considering the usual practice that a ballistic missile is designed to perform maneuvers in only the longitudinal direction, a dynamic model describing motion in the vertical plane is required.

The kinematic equations considered in this study can be represented as

$$\frac{dx}{dt} = v(t)\cos\gamma(t) \tag{1}$$

$$\frac{dh}{dt} = v(t)\sin\gamma(t) \tag{2}$$

where v is the velocity of the missile, γ is the vertical flight path angle, x is the horizontal displacement defined to be positive in the direction from the launch point to the target, and h is the altitude of the missile. The dynamic

equations for the missile can be represented as

$$\frac{dv}{dt} = \frac{T(t) - D(v,\alpha)}{m(t)} - g(h(t))\sin\gamma(t) + \Omega_e^2 r(t)\cos\phi(t)(\sin\gamma(t)\cos\phi(t) - \cos\gamma(t)\sin\phi(t)\sin\gamma(t)) \tag{3}$$

$$\frac{d\gamma}{dt} = \frac{L(t)\cos\sigma(t)}{m(t)v(t)} - \frac{g(h(t))}{v(t)}\cos\gamma(t) + \frac{v(t)}{r(t)}\cos\gamma(t) + 2\Omega_e^2\cos\phi(t)\cos\psi(t) + \frac{\Omega_e^2 r(t)}{v(t)}\cos\phi(t)(\cos\gamma(t)\cos\phi(t) + \sin\gamma(t) + \sin\phi(t)\sin\psi(t)) \tag{4}$$

where σ is the bank angle, ϕ is the roll angle, ψ is the yaw angle, r denotes the distance of the missile from the Earth center, m denotes the vehicle mass, Ω_e is the Earth's rotation rate, and g is the gravitational acceleration. D and L are the drag force and the lift force, respectively, which can be represented as

$$D = C_D(v,\alpha)\left(\frac{1}{2}\rho(h(t))v(t)^2\right)S \tag{5}$$

$$L = C_L(v,\alpha)\left(\frac{1}{2}\rho(h(t))v(t)^2\right)S \tag{6}$$

where ρ is the density of the atmosphere, S is the reference area of the missile, and C_D and C_L are the aerodynamic coefficients. Earth rotation and the Coriolis effect terms are not essential for the proposed framework. Therefore, the Earth is assumed to be nonrotating, and the Coriolis effect is neglected in this study. Note that the system considered in this study is a gliding ballistic missiles after burnout, and therefore, thrust T is treated as zero. Furthermore, term $\frac{v(t)}{r(t)}$ is negligible because $r(t)$ is much larger than $v(t)$. The roll angle, bank angle, and yaw angle are assumed to be zero because the gliding ballistic missile after burnout flies in the vertical plane without movement in the horizontal direction to improve the viability and increase the performance. Then, the dynamic equations (3) and (4) in the burnout condition can be rewritten as follows:

$$\frac{dv}{dt} = \frac{-D(v,\alpha)}{m} - g(h(t))\sin\gamma(t) \tag{7}$$

$$\frac{d\gamma}{dt} = \frac{L(t)}{mv(t)} - \frac{g(h(t))}{v(t)}\cos\gamma(t) \tag{8}$$

C. Proposed Framework

The actual environment in which missiles operate is close to the mathematical model but is not exactly the same. Therefore, the missile flies along a different trajectory from the one expected before flight. If it is possible to find a trajectory satisfying the terminal velocity constraint while updating the information in real time, then the velocity error can be reduced.

The method proposed in this study updates the trajectory to satisfy the terminal velocity constraint by using the information of the current missile location as well as the target location during the flight. Fig. 1 shows the block diagram of the gliding missile system considered in this study, which includes the schematic configuration of the proposed framework in the guidance block.

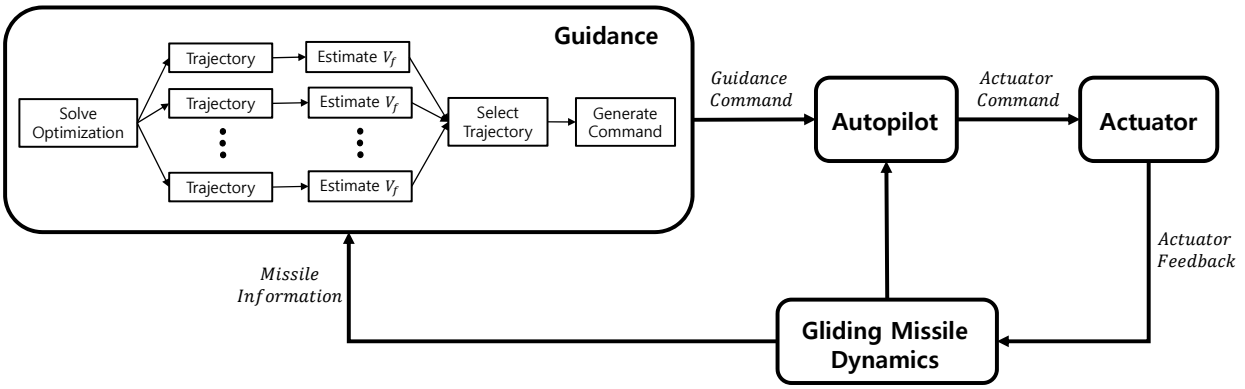

Fig. 1: Schematic Diagram of the Framework

A constrained optimization problem is solved to generate trajectories. The objective function of the optimization is set to be a quadratic function in this study. The proposed optimal problem is solved using the sequential quadratic programming method. The objective function can be expressed as follows:

$$\min_{\underline{\mathbf{C}}} J = K^2 + R \int_{x_i}^{x_f} \left(\frac{d^2 h(x)}{dx^2} \right)^2 dx \tag{9}$$

where the first term K can be selected considering some preference to the specific shape of the trajectory, and $\underline{\mathbf{C}}$ is the optimization variable, which will be explained in the subsequent section. For example, K can be chosen to place a lower penalty for a path with its flight path angle closer to a specific profile so that the trajectory will be shaped through the optimization. In a similar way, the trajectories can be generated for the missile to maneuver mainly around a specific altitude or to follow a reference altitude profile.

The second term is related to the curvature of the trajectory. Because curvature refers to a rate of change indicating the degree of curvature of a curve, the second term in the performance index (9) affects the curved shape of the generated trajectory. A positive weighting factor, R, in the objective function plays the role of a tunable parameter to produce various trajectories. With the assumption made in this study, energy should be managed by maneuvering the missile on the vertical plane. In other words, a missile with sufficient energy should generate a large curvature to dissipate the energy through an additional maneuver. On the other hand, a missile with a lack of energy should fly as straight as possible toward the target to preserve its energy. In this way, the magnitude of trajectory curvature affects the energy management of the missile, and various trajectories can be obtained by tuning R.

III. Trajectory Planning Framework

A. Trajectory Generation

1) Trajectory Equation: For the flight trajectory in the vertical plane, altitudes h are expressed as the following polynomial function of downrange x:

$$\begin{aligned} h(x) &= a_n x^n + a_{n-1}x^{n-1} + \cdots + a_1 x + a_0 \\ &= \begin{pmatrix} a_n & a_{n-1} & \cdots & a_0 \end{pmatrix} \begin{pmatrix} x^n \\ x^{n-1} \\ \vdots \\ x^0 \end{pmatrix} \\ &= \underline{\mathbf{C}}^T \underline{\mathbf{\Phi}}(x) \end{aligned} \tag{10}$$

where n is the maximum degree of the polynomial, a_i's are the coefficients of the trajectory polynomial equation, $\underline{\mathbf{C}}$ is the vector of coefficients, and $\underline{\mathbf{\Phi}}$ is the basic formation vector of the downrange parameter x. The trajectory generation part aims to find a $\underline{\mathbf{C}}$ that satisfies the constraints of the trajectory.

2) Quadratic Programming Formulation: Minimizing the objective function defined in (9) can result in various types of trajectories by adjusting R. By applying (10) to (9), the objective function can be represented as follows:

$$\begin{aligned} \min_{\underline{\mathbf{C}}} J &= K^2 + R\int_{x_i}^{x_f} \left(\frac{d^2h(x)}{dx^2}\right)^2 dx \\ &= K^2 + R\underline{\mathbf{C}}^T \mathbf{DEFE}^T \mathbf{D}^T \underline{\mathbf{C}} \\ &= \underline{\mathbf{C}}^T (R\mathbf{DEFE}^T\mathbf{D}^T)\underline{\mathbf{C}} + K^2 \end{aligned} \tag{11}$$

where $\mathbf{D}$, $\mathbf{E}$, and $\mathbf{F}$ are $(n+1)$ by $(n+1)$ matrices, x_i is the initial downrange, x_f is the final downrange, and the upper subscript T refers to the transpose of a matrix. The details of the derivation of the matrices $\mathbf{D}$, $\mathbf{E}$, and $\mathbf{F}$ can be found in the appendix.

Equality constraints can be formulated by the waypoint information as

$$h_i = h(x_i) = \underline{\mathbf{C}}^T \underline{\mathbf{\Phi}}(x_i) \tag{12}$$

$$h_f = h(x_f) = \underline{\mathbf{C}}^T \underline{\mathbf{\Phi}}(x_f) \tag{13}$$

$$\tan(\gamma_i) = \frac{dh(x_i)}{dx} = \underline{\mathbf{C}}^T \mathbf{D}\underline{\mathbf{\Phi}}(x_i) \tag{14}$$

$$\tan(\gamma_f) = \frac{dh(x_f)}{dx} = \underline{\mathbf{C}}^T \mathbf{D}\underline{\mathbf{\Phi}}(x_f) \tag{15}$$

On the other hand, inequality constraints can be formulated by considering the mission constraints. In this study, the minimum altitude h_{min} and the maximum altitude h_{max} of the missile are considered as follows:

$$h_{min} \leq h(x) = \underline{\mathbf{C}}^T \underline{\mathbf{\Phi}}(x) \leq h_{max}, \quad \forall x \tag{16}$$

B. Dynamic Propagation

1) Model Reduction: Similar to the trajectory equation, velocity v and vertical flight path angle γ can be described by the downrange x using the kinematic and dynamic models described in Sec. II-B as follows:

$$\frac{dv}{dx} = \frac{\frac{dv}{dt}}{\frac{dx}{dt}} = \frac{-D(x,\alpha)}{mv(x)\cos\gamma(x)} - \frac{g(h(x))}{v(x)}\tan\gamma(x) \tag{17}$$

$$\frac{d\gamma}{dx} = \frac{\frac{d\gamma}{dt}}{\frac{dx}{dt}} = \frac{L(x,\alpha)}{mv(x)^2\cos\gamma(x)} - \frac{g(h(x))}{v(x)^2} \tag{18}$$

Considering the velocity of the ballistic missile, it is reasonable to assume that $g(x) \ll v(x)^2$ and the second term of (18) can be neglected. Therefore, (18) can be rewritten as follows:

$$\frac{d\gamma}{dx} = \frac{L(x)}{mv(x)^2\cos\gamma(x)} = \frac{\rho(h(x))C_L(v,\alpha)S}{2m\cos\gamma(x)} \tag{19}$$

Since the derivative of the trajectory with respect to x has the same meaning as the tangent of the flight path angle, γ and its derivative can be obtained as follows:

$$\gamma(x) = \arctan\left(\frac{dh(x)}{dx}\right) = \arctan(\underline{\mathbf{C}}^T\mathbf{D}\underline{\mathbf{\Phi}}(x)) \tag{20}$$

Comparing (19) and (20) yields the following equation.

$$\frac{\rho(h(x))C_L(v,\alpha)S}{2m\cos\gamma(X)} = \frac{1}{1+\left(\frac{dh(x)}{dx}\right)^2}\frac{d^2h(x)}{dx^2} \tag{21}$$

Then, $C_L(v,\alpha)$ can be expressed in terms of altitude and its derivatives as follows:

$$C_L(v,\alpha) = \frac{1}{1+\left(\frac{dh(x)}{dx}\right)^2}\left(\frac{d^2h(x)}{dx^2}\right)\frac{2m\cos\gamma(x)}{\rho(h(x))S} \tag{22}$$

or

$$C_L(v,\alpha) = \frac{1}{1+(\underline{\mathbf{C}}^T\mathbf{D}\underline{\mathbf{\Phi}}(x))^2}(\underline{\mathbf{C}}^T\mathbf{D}\mathbf{E}\underline{\mathbf{\Phi}}(x))\frac{2m\cos\gamma(x)}{\rho(h(x))S} \tag{23}$$

Because m and S are known missile characteristics, the lift coefficient C_L at altitude $h(x)$ and a specific down range x can be estimated. Considering (6), the relationship between the drag force and lift force can be established as follows:

$$\frac{L(v,\alpha)}{D(v,\alpha)} = \frac{C_L(v,\alpha)}{C_D(v,\alpha)} = LD_{ratio} \tag{24}$$

where LD_{ratio} is the lift-to-drag ratio. If the aerodynamic model is known, v and α can be estimated by comparing the values of the secondary table of the lift coefficient C_L. Then, the drag coefficient C_D can be estimated. Because the lift-to-drag ratio of the missile is known, $D(v, \alpha)$ can be computed as

$$D(v,\alpha) = \frac{1}{LD_{ratio}} L(v,\alpha) = \frac{1}{LD_{ratio}} \left(C_L\left(v,\alpha\right) \left(\frac{1}{2} \rho(h(x)) v^2 \right) S \right) \tag{25}$$

Therefore, the derivative of v with respect to x can be calculated as follows:

$$\begin{aligned} \frac{dv}{dx} &= \frac{-D(x,\alpha)}{mv(x)\cos\gamma(x)} - \frac{g(h(x))}{v(x)} \tan\gamma(x) \\ &= \frac{-\rho(h(x))v(x)SC_L(v,\alpha)}{2m\cos\gamma(x) LD_{ratio}} - \frac{g(h(x))}{v(x)} \tan\gamma(x) \end{aligned} \tag{26}$$

In summary, (19) and (26) with (23) and (24) describe the dynamic model with respect to the downrange.

2) Prediction of Terminal Velocity: The terminal velocity of the trajectory can be predicted by applying a simple numerical integration of (26). In this study, the Euler method is utilized, which is more efficient than high-order integration methods such as the 4th-order Runge-Kutta method even if it has low accuracy.

The terminal velocity can be estimated for a given path as

$$v(x_f) = v(x_i) + \int_{x_i}^{x_f} \left(\frac{dv\left(x\right)}{dx} \right) dx \approx v(x_i) + \sum_j \left. \frac{dv\left(x\right)}{dx} \right|_{x_j} \Delta x_j \tag{27}$$

Note that the step size Δx_j that affects both the computational time and the predictive accuracy can be determined by considering a fixed time increment Δt as follows:

$$\Delta x_j = v(x_j)\cos(\gamma(x_j))\Delta t \tag{28}$$

The proposed framework is summarized as follows. First, trajectories are generated, and the terminal velocity is efficiently calculated for each trajectory. The trajectory prescribes the altitude as a function of downrange. The velocity and the flight path angle are the variables of system dynamics represented by the downrange. Assuming that the aerodynamic model is known, the lift and drag forces are calculated from the geometrical properties of the path. The terminal velocity can be obtained by propagating a scalar differential equation for the velocity along the given path. The step size for numerical integration adjusts the trade-off between computational time and predictive accuracy. Fig. 2 shows the flowchart of the trajectory planning framework with the described equation. Fig. 2 shows the process of 'Guidance' block in Fig. 1.

Since the proposed prediction algorithm is calculated as a definite integral, divergence occurring the general guidance algorithm do not need to consider. If the gliding missile has a much different energy than expected, the proposed prediction algorithm will not work normally.

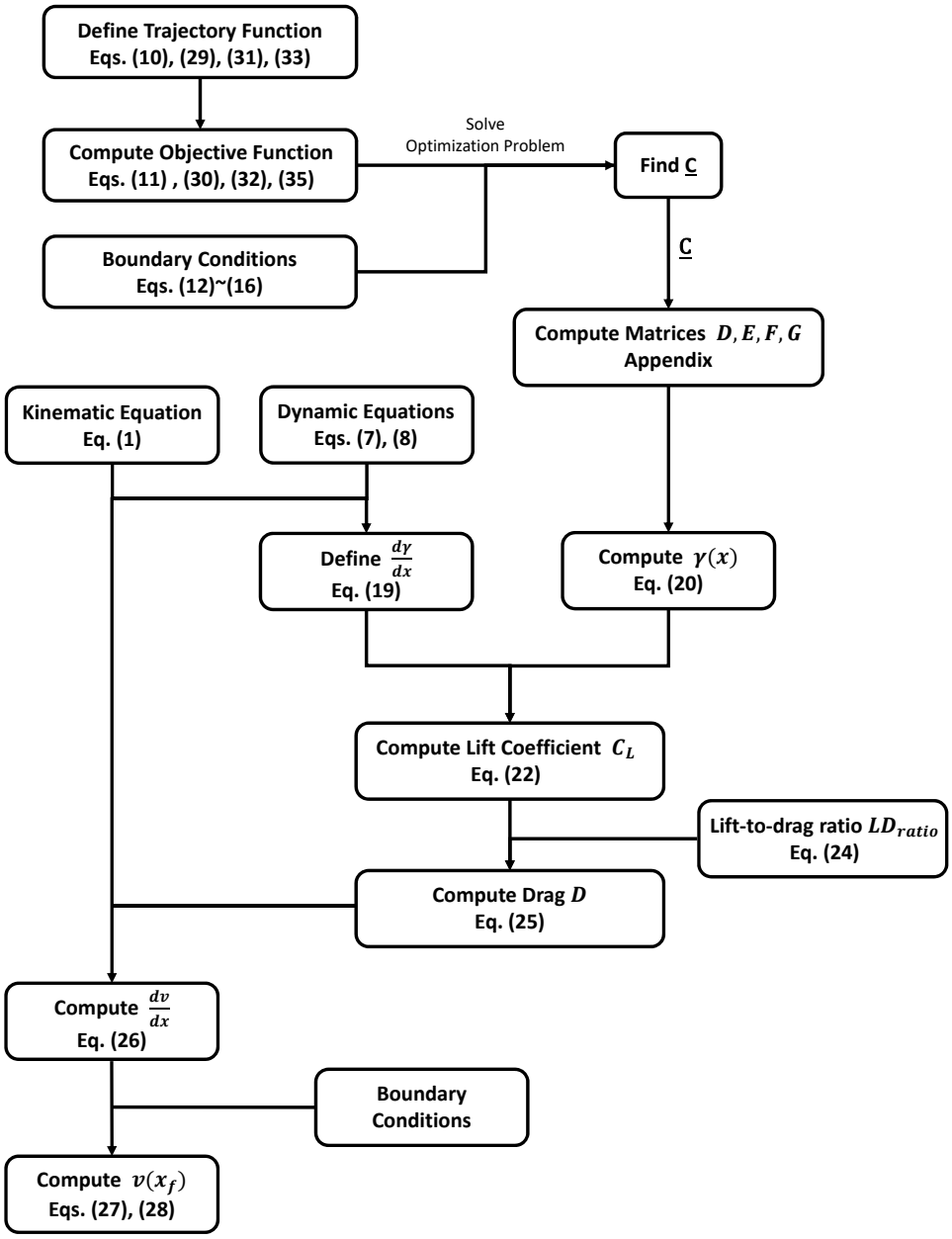

Fig. 2: Flowchart of the Trajectory Planning Framework

IV. Performance Index

In this section, three types of performance indices are explained. Each performance index differs by the term K in the objective function, which is represented in (11). Note that equality and inequality constraints are already described in Sec. III-A2.

A. Minimization of Terminal Velocity Direction Error

The objective function in this case is defined as follows:

$$\min_{\underline{\mathbf{C}}} J = (\tan\gamma_f - \tan\gamma_{des})^2 + R\int_{x_i}^{x_f}\left(\frac{d^2h(x)}{dx^2}\right)^2 dx \tag{29}$$

The first term in (29) is set to satisfy the direction of the terminal velocity constraint, where γ_{des} is the desired vertical flight path angle at the first point. The tangent function is used instead of the flight path angle to utilize the definition where the derivative of the trajectory has the same meaning as the tangent of the vertical flight path angle. Equation (29) can be rewritten using (11) and the definition of matrix $\mathbf{D}$ as follows:

$$\begin{aligned}\min_{\underline{\mathbf{C}}} J &= (\underline{\mathbf{C}}^T\mathbf{D}\underline{\mathbf{\Phi}}(x_f) - \tan\gamma_{des})^2 + R\underline{\mathbf{C}}^T\mathbf{DEFE}^T\mathbf{D}^T\underline{\mathbf{C}} \\ &= \frac{1}{2}\underline{\mathbf{C}}^T 2[(\mathbf{D}\underline{\mathbf{\Phi}}(x_f)\underline{\mathbf{\Phi}}(x_f)^T\mathbf{D}^T + R\mathbf{DEFE}^T\mathbf{D}^T)]\underline{\mathbf{C}} + \underline{\mathbf{C}}^T(-2\tan\gamma_{des}\mathbf{D}\underline{\mathbf{\Phi}}(x_f)) + (\tan\gamma_{des})^2 \\ &:= \frac{1}{2}\underline{\mathbf{C}}^T\mathbf{Q}_1\underline{\mathbf{C}} + \underline{\mathbf{C}}^T\underline{\mathbf{f}}_1 + (\tan\gamma_{des})^2\end{aligned} \tag{30}$$

B. Minimization of Deviation From a Specific Altitude

The terminal velocity of the missile is greatly affected by the flight range and flight time. The velocity reduction due to the aerodynamic force varies because the aerodynamic force depends on the altitude. In this case, the objective function is set to fly around a specific altitude (h_{ref}) as follows:

$$\min_{\underline{\mathbf{C}}} J = \int_{x_i}^{x_f}(h(x) - h_{ref})^2 dx + R\int_{x_i}^{x_f}\left(\frac{d^2h(x)}{dx^2}\right)^2 dx \tag{31}$$

The first term in (31) is set to satisfy the altitude constraint. Now, (31) can be expanded as follows:

$$\begin{aligned}\min_{\underline{\mathbf{C}}} J &= \int_{x_i}^{x_f}(\underline{\mathbf{C}}^T\underline{\mathbf{\Phi}}(x) - h_{ref})^2 dx + R\underline{\mathbf{C}}^T\mathbf{DEFE}^T\mathbf{D}^T\underline{\mathbf{C}} \\ &= \frac{1}{2}\underline{\mathbf{C}}^T 2(\mathbf{F} + R\mathbf{DEFE}^T\mathbf{D}^T)\underline{\mathbf{C}} + \underline{\mathbf{C}}^T(-2h_{ref}\mathbf{G}) + (x_f - x_i)h_{ref}^2 \\ &:= \frac{1}{2}\underline{\mathbf{C}}^T\mathbf{Q}_2\underline{\mathbf{C}} + \underline{\mathbf{C}}^T\underline{\mathbf{f}}_2 + (x_f - x_i)h_{ref}^2\end{aligned} \tag{32}$$

C. Minimization of Deviation From a Preference Path

The objective function can be constructed to generate new trajectories around a given reference that was obtained previously with an offline optimization approach. The computational burden of this case may be low because the search area is reduced by the offline setting. The flight trajectory differs from the expected trajectory because the real environment is different from the expected environmental model. Even if an error in the trajectory occurs due

to the uncertainty of the environment, a new trajectory can be found in a trust region near the optimal trajectory obtained in the previous step. Even though the trajectory is optimized using the energy management waypoint planning framework in advance [1], the obtained trajectory is not optimal due to uncertainty. Therefore, an iterative process is needed by utilizing the current flight information to obtain a new optimal trajectory in the vicinity of the previous optimal trajectory.

The objective function, in this case, is defined as follows:

$$\min_{\underline{\mathbf{C}}} J = ((h(x) - g(x))^2 + R \int_{x_i}^{x_f} \left(\frac{d^2 h(x)}{dx^2} \right)^2 dx \tag{33}$$

where $g(x)$ is the optimal trajectory of the previous step. In this case, $g(x)$ is obtained by scenario A of $x_{TGT} = 120km$ in [1]. $g(x)$ can be constructed as follows:

$$\begin{aligned} g(x) &= b_n x^n + b_{n-1} x^{n-1} + \cdots + b_1 x + b_0 \\ &= \begin{pmatrix} b_n & b_{n-1} & \cdots & b_0 \end{pmatrix} \begin{pmatrix} x^n \\ x^{n-1} \\ \vdots \\ x^0 \end{pmatrix} \\ &= \underline{\mathbf{B}}^T \underline{\mathbf{\Phi}}(x) \end{aligned} \tag{34}$$

The first term in (33) is to find the optimal trajectory in the vicinity of $g(x)$. Now, (33) can be expressed as follows:

$$\begin{aligned} \min_{\underline{\mathbf{C}}} J &= \int_{x_i}^{x_f} (\underline{\mathbf{C}}^T \underline{\mathbf{\Phi}}(x) - \underline{\mathbf{B}}^T \underline{\mathbf{\Phi}}(x))^2 dx + R \underline{\mathbf{C}}^T \mathbf{DEFE}^T \mathbf{D}^T \underline{\mathbf{C}} \\ &= \underline{\mathbf{C}}^T \mathbf{F} \underline{\mathbf{C}} - \underline{\mathbf{C}}^T \mathbf{F} \underline{\mathbf{B}} - \underline{\mathbf{B}}^T \mathbf{F} \underline{\mathbf{C}} + \underline{\mathbf{B}}^T \mathbf{F} \underline{\mathbf{B}} + R \underline{\mathbf{C}}^T \mathbf{DEFE}^T \mathbf{D}^T \underline{\mathbf{C}} \\ &= \frac{1}{2} \underline{\mathbf{C}}^T 2(\mathbf{F} + R\mathbf{DEFE}^T \mathbf{D}^T) \underline{\mathbf{C}} + \underline{\mathbf{C}}^T (-\mathbf{F} - \mathbf{F}^T) \underline{\mathbf{B}} + \underline{\mathbf{B}}^T \mathbf{F} \underline{\mathbf{B}} \\ &:= \frac{1}{2} \underline{\mathbf{C}}^T \mathbf{Q}_3 \underline{\mathbf{C}} + \underline{\mathbf{C}}^T \underline{\mathbf{f}}_3 + \underline{\mathbf{B}}^T \mathbf{F} \underline{\mathbf{B}} \end{aligned} \tag{35}$$

V. Numerical Simulations

Numerical simulations are performed to verify the performance of the proposed algorithm. Different simulation scenarios are considered with various formulation choices, including the form of the objective function (see Sec. V-A), the constraints, the maximum degree of the polynomial trajectory (see Sec. V-B), and the time step for velocity prediction (see Sec. V-C). Additionally, the performance of the proposed algorithm in the presence of modeling uncertainties is studied in Sec. V-E.

The energy management waypoint planning framework presented in [1] is adopted to provide realistic problem data for the validation of the proposed framework. Waypoints 1 and 2 are the initial point and final point, respectively, used in scenario A in which x_{TGT} is set to be $120km$. Table I summarizes the waypoint information as the initial point and final point.

The weighting factor R in (9) is formulated as the power of 10 as follows:

$$R = 10^r \tag{36}$$

TABLE I: Initial Point and Final Point.

	Down Range	Height	Velocity	Flight Path Angle
Initial Point	$35.24km$	$12.74km$	$834.37m/s$	$-0.05deg$
Final Point	$98.84km$	$7.14km$	$384.29m/s$	$-28.00deg$

where the exponent r is a tunable parameter. Let us define V_{err} as the velocity error at the final point, i.e.,

$$V_{err} = V_{des} - V_{final_{est}} \tag{37}$$

where V_{des} is the desired velocity at the final point, and $V_{final_{est}}$ is the estimated terminal velocity.

Simulations are performed using MATLAB on a computer with an Intel i5-7300 CPU @ 2.5 GHz and 8 GB RAM.

A. Various Objective Functions

Each case uses the performance index, which is explained in Sec. IV. Additionally, the degree of polynomial n is set to be 9, and the propagation step size Δx is defined by choosing $\Delta t = 1$ sec.

1) Example Case 1: The performance index described in Sec. IV-A is used. The results are shown by changing r with the interval of 0.1 units from -9 to -4. Fig. 3a) and 3b) show the simulation results of this case. Fig. 3c) shows the velocity error with respect to r. If the value of r is excessively small or large, which means that the value of R is extreme, numerical instability occurs. In this case, it is judged that the optimization has failed and is not shown in Fig. 3c). Fig. 3a) shows that various trajectories are generated according to the change in r. The velocity profile is illustrated for each trajectory, and each terminal velocity may be predicted, as shown in Fig. 3b) and 3c). By analyzing the results of Fig. 3c), the guidance law can give the command to follow the trajectory with the smallest velocity error.

2) Example Case 2: In this example case, the objective function and constraints in Sec. IV-B are used. The results are shown by changing r with an interval of 0.1 units from -7 to -3 and h_{ref} with the interval of 0.5 km units from 7 km to 20 km. To better understand the tendency, the results obtained with various desired attitudes h_{ref} for a fixed weighting $r = -5$ are shown in Figs. 4a) and 4b). The legends represent the desired altitude h_{ref}. Fig. 4c) shows the velocity error with respect to r and h_{ref}. Fig. 4d) shows the values of r and h_{ref} when the velocity error is zero. At least one solution can be found for each h_{ref}. Trajectories satisfying a given constraint are generated in various ways, as shown in Fig. 4a). The velocity profile of each trajectory is different, as shown in Fig. 4b), and therefore, the terminal velocity error is predicted differently. In the $r = -5$ case, flying at an altitude of $12km$ provides the best result.

3) Example Case 3: The contents explained in Sec. IV-C are applied. The results are shown by changing r with an interval of 0.1 units from -5 to 0. Figs. 5a) and 5b) show the simulation results of this case. The missile maneuvers at low altitudes as the value of r approaches -5 and at high altitudes as the value of r approaches 0. Additionally, the generated optimal trajectory is similar to $g(x)$ as r approaches 0. Fig. 5c) represents the velocity error with respect to r.

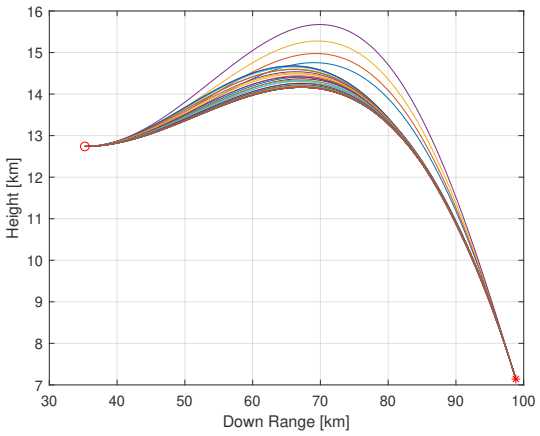

(a) Trajectory of the missile (Case 1).

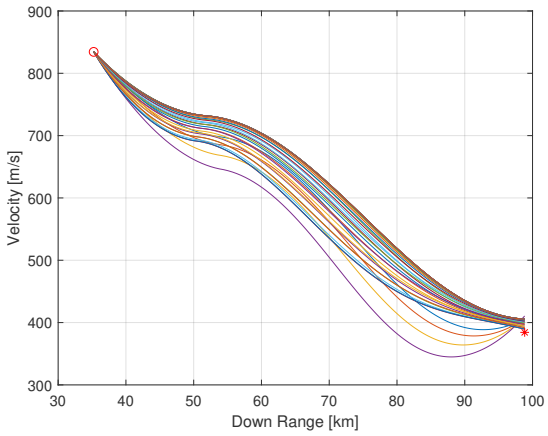

(b) Velocity of the missile (Case 1).

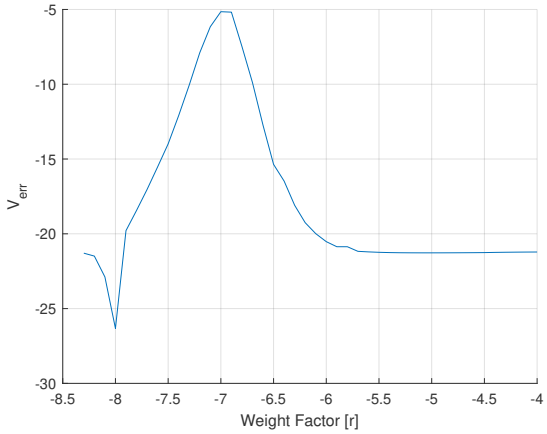

(c) Velocity error (Case 1).

Fig. 3: Simulation Results for Case 1

4) Selected Trajectory of Each Case: The best trajectory is selected, which has the smallest velocity error in each case. In Case 2, R is also considered. Table II summarizes the results of each case.

TABLE II: Selected trajectory of each case

	r	h_{ref}	V_{err}	$Time: TrjGen$	$Time: DynPro$
Case 1	-7	–	5.1 m/s	0.012 sec	0.024 sec
Case 2	-5.2	12.5 km	1.8 m/s	0.011 sec	0.024 sec
Case 3	-4	–	2.9 m/s	0.013 sec	0.029 sec

The velocity error from the desired velocity shows a value of approximately within $5m/s$ for the conditions considered in this study. Considering the velocity of a ballistic missile that exceeds the hypersonic speed, the error is very small. If r is designed more closely, the velocity error will decrease. The execution time of each algorithm is

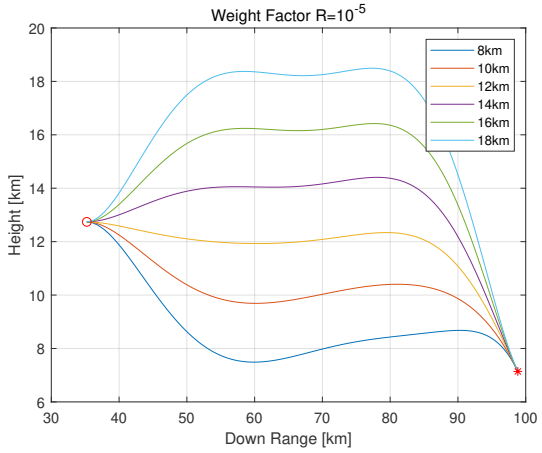

(a) Trajectory of the missile (Case 2).

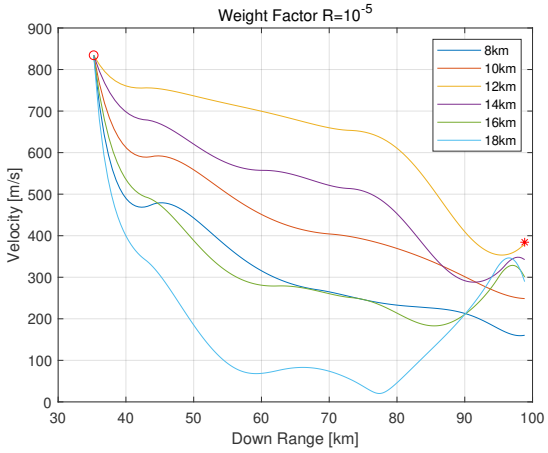

(b) Velocity of the missile (Case 2).

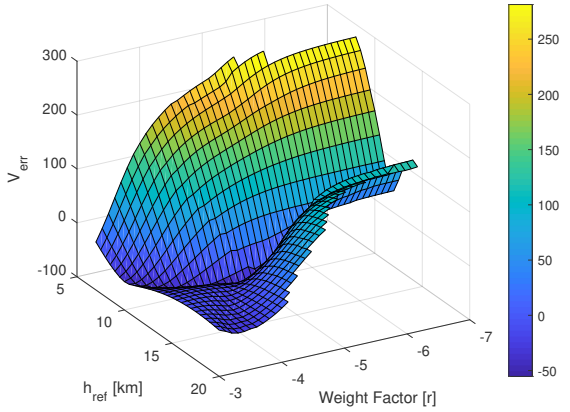

(c) Velocity error (Case 2).

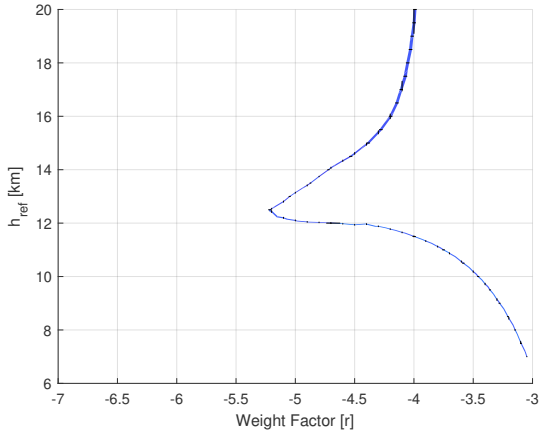

(d) r and h_{ref} when velocity error is zero (Case 2).

Fig. 4: Simulation Results for Case 2

approximately 0.01 sec, which can be implemented in real time. Figs. 6a) and 6b) show the trajectory and velocity of the selected cases.

B. Various n

The maximum degree of trajectory can affect the shape of the optimal trajectory and thus the estimated terminal velocity. To analyze the influence of the degree of trajectory, n is changed with the interval of 1 units from 3 to 10. The objective function and constraints are the same as in Sec. V-A3, r is set as -4, and the step size Δx for speed dynamics propagation is defined by Δt being 1 sec.

Figs. 7a)–7c) show the results obtained by changing n. Different trajectories are generated when n is 3 or 4. However, there is no significant difference when n is greater than or equal to 5. In other words, if n is less than 5, a simple trajectory shape can be generated. If n is greater than or equal to 5, a trajectory with a similar shape can be obtained, which means increasing n further is unnecessary.

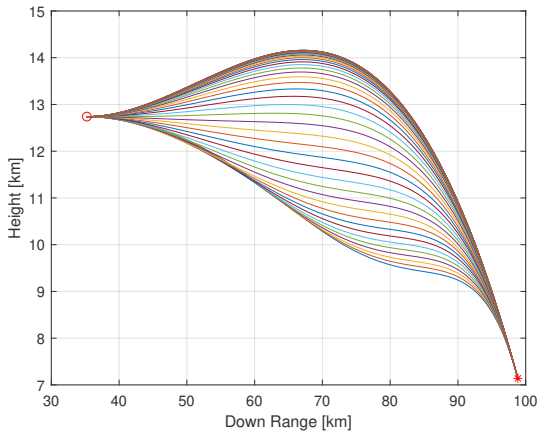

(a) Trajectory of the missile (Case 3).

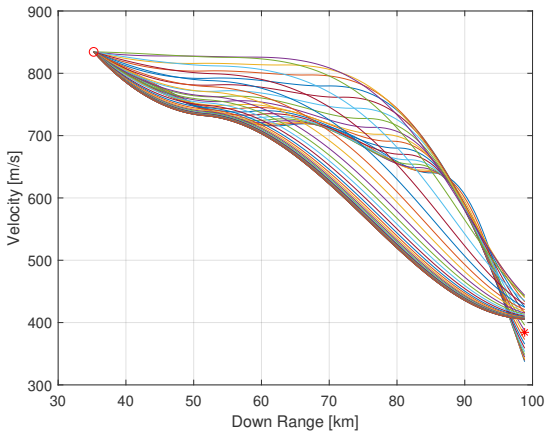

(b) Velocity of the missile (Case 3).

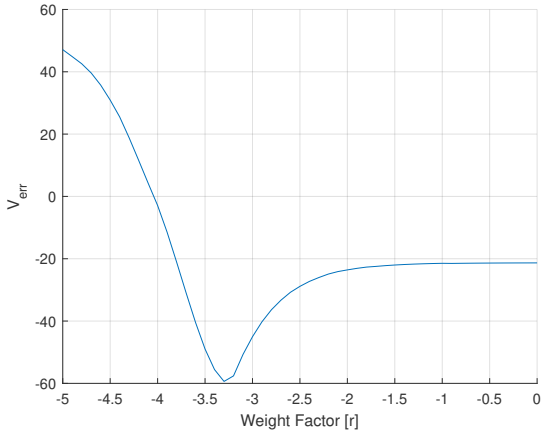

(c) Velocity error (Case 3).

Fig. 5: Simulation Results for Case 3

C. Various Δt

To update the trajectory, Δx is needed as an interval when performing the propagation. The update interval directly affects the computational time and the results of estimation terminal velocity, as shown in (27) and (28). When updating the trajectory information in the propagation, the final updated point may not be an exact point due to the discretization. In this case, the terminal speed at the final point is predicted through the following process. First, Δx is defined by the current velocity v_i, flight path angle γ_i, and Δt. Second, the next downrange x_{i+1} and velocity v_{i+1} are updated by the dynamic propagation algorithm. If the next downrange x_{i+1} is greater than the downrange of final point x_f, the iteration stops, and the terminal velocity is estimated by linear interpolation as

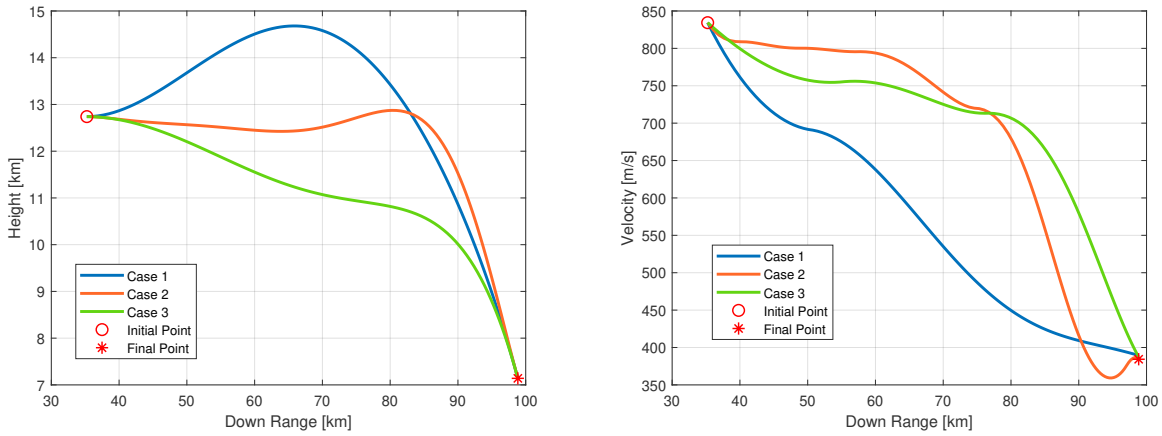

(a) Trajectory of the missile (Best cases).

(b) Velocity of the missile (Best cases).

Fig. 6: Summary of Trajectory Planning Results

follows:

$$\begin{aligned} v_f &= v_i + \Delta v_i \frac{\Delta x_f}{\Delta x_i} \\ &= v_i + (v_{i+1} - v_i) \frac{x_f - x_i}{x_{i+1} - x_i} \end{aligned} \tag{38}$$

where the variables are defined as shown in Fig. 8.

To investigate the influence of time increment, Δt is changed from 0.001 sec to 2.0 sec with an increment of 0.001 sec. The objective function and constraints are the same as in Sec. V-A2. Additionally, r, h_{ref}, and n are set as -4.5, $12\ km$, and 9, respectively. Figs. 9a) and 9b) represent the results obtained by changing Δt. Note that only three representative results are shown in Figs. 9a) and 9b). There is no significant difference in the trajectory and velocity profiles by changing Δt. Fig. 9c) shows the difference in velocity error for various Δt. Theoretically, the accuracy increases as Δt decreases. However, the difference in velocity error is less than $10 m/s$, as shown in Fig. 9c), which is a small value considering the velocity of the ballistic missile.

A chattering phenomenon in Fig. 9c) comes from the nonmonotonic characteristics of Δx_f. The computation time for trajectory generation and dynamic propagation is analyzed for each Δt, as shown in Fig. 9d). If Δt is greater than $0.4 sec$, the computation time for both trajectory generation and dynamic propagation is less than $0.01 sec$. Considering the results shown in Figs. 9a) and 9b), the proposed framework produces similar trajectories even if Δt is relatively large. Therefore, one can conclude that the proposed algorithm can efficiently predict the terminal velocity of the missile.

D. Multiple Waypoints in Real-time

Simulations are performed for the case with multiple waypoints between the initial and final positions. The waypoint information is assumed to be obtained using the energy management waypoint planning framework [1], while the constraints of missiles and missions are given. Specifically, the waypoint information of scenario A in [1]

is considered. With the first waypoint as the initial point and the third waypoint as the final point, the proposed framework is utilized to produce the trajectory through the second waypoint. Table III describes the information of each point.

TABLE III: Initial Point, Intermediate Point and Final Point.

	Downrange	Height	Velocity	Flight Path Angle
Initial Point	$35.24km$	$12.74km$	$834.37m/s$	$-0.05deg$
Intermediate Point	$98.84km$	$7.14km$	$384.29m/s$	$-28.00deg$
Final Point	$104.80km$	$5.80km$	$365.00m/s$	$-28.00deg$

Figs. 10a) and 10b) show the simulation results, in which a line is the profile of the missile, a circle denotes the initial point, a square denotes the final point, and a diamond denotes the intermediate waypoint.

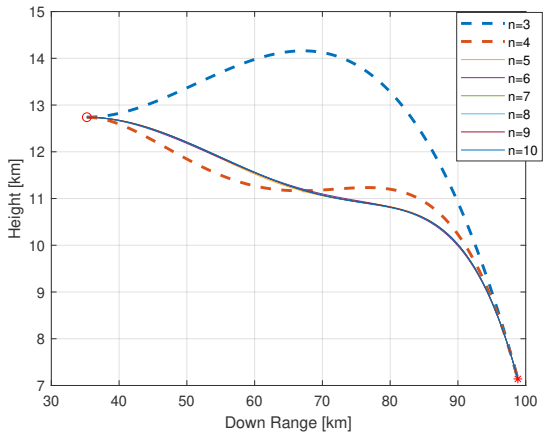

(a) Trajectory of the missile by varying n.

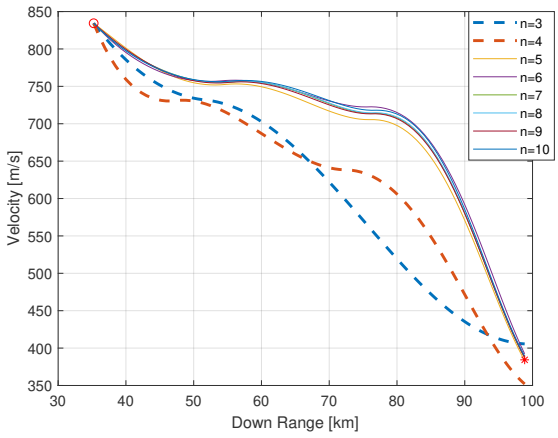

(b) Velocity of the missile by varying n.

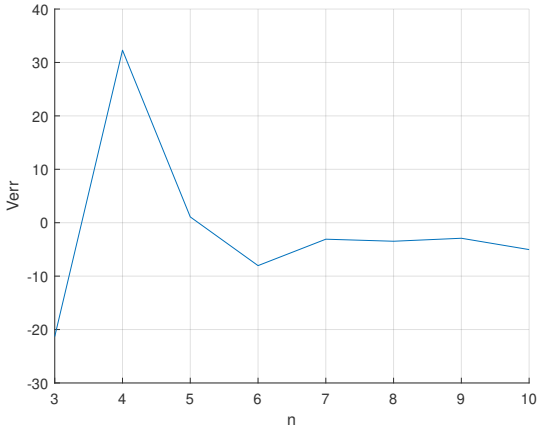

(c) Velocity error by varying n.

Fig. 7: Simulation Results with Various n

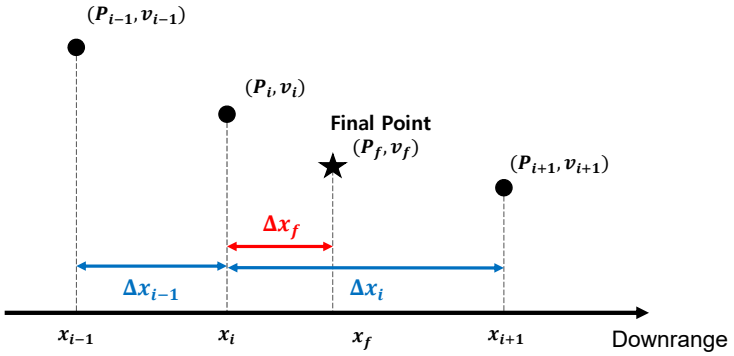

Fig. 8: Propagation point near the final point.

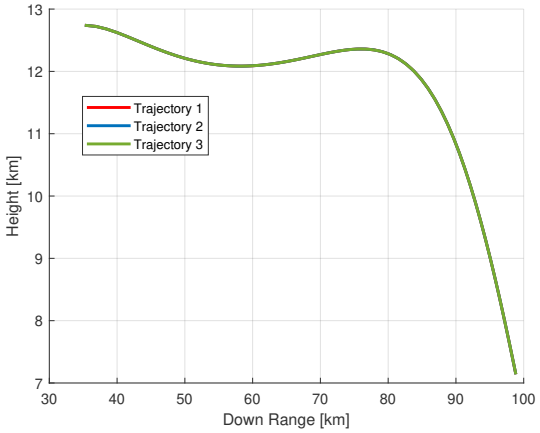

(a) Trajectory of the missile by varying Δt.

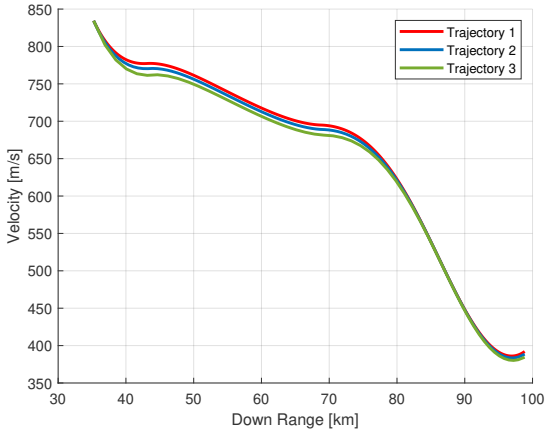

(b) Velocity of the missile by varying Δt.

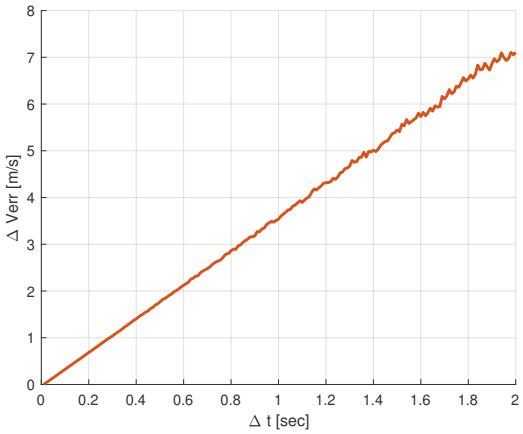

(c) Difference of velocity error by varying Δt.

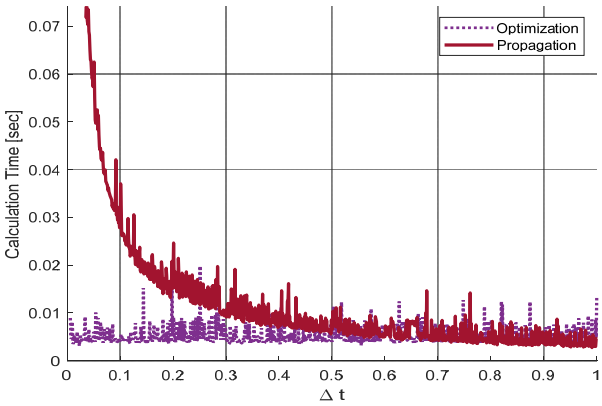

(d) Calculation time by varying Δt.

Fig. 9: Simulation Results with Various Δt

As shown in Fig. 10a), the vehicle maneuvers well from the initial point to the final point through the intermediate point. The velocity error at the path point is $0.7\ m/s$, and at the final point is $-1.5\ m/s$. The missile flies according

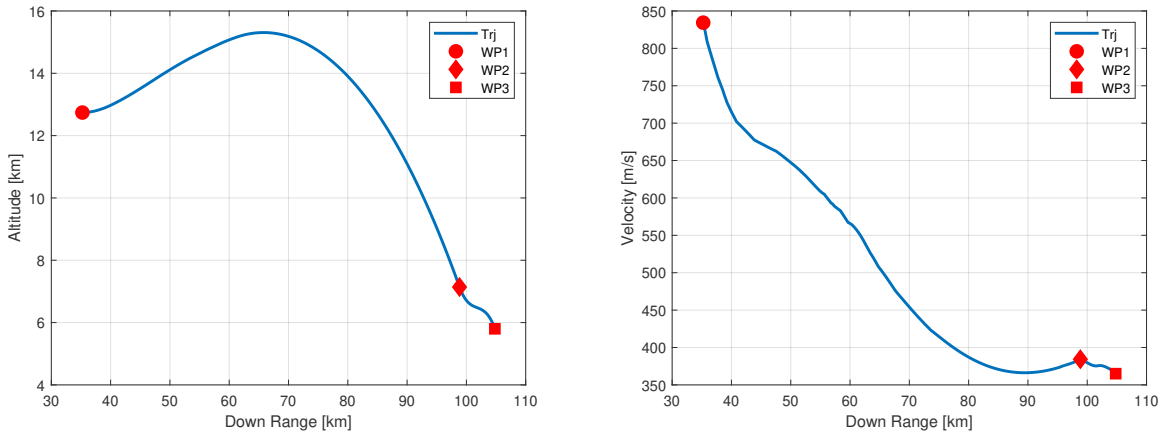

(a) Trajectory of the missile from Waypoint 1 to Waypoint 3. (b) Velocity of the missile from Waypoint 1 to Waypoint 3.

Fig. 10: Simulation Results with Multiple Waypoints

to the purpose of the proposed framework.

E. Influence of Uncertainty in Real Time

Real-time simulations are conducted considering uncertainty in the environmental model. The objective function and constraints are the same as in Sec. V-A1. To reflect uncertainty, random values within a certain range are added to the position (x, h), velocity (v), and flight path angle (γ) of the missile at each time step as follows:

$$x(i+1) = x(i) + x_u(i) \tag{39}$$

$$h(i+1) = h(i) + h_u(i) \tag{40}$$

$$v(i+1) = v(i) + v_u(i) \tag{41}$$

$$\gamma(i+1) = \gamma(i) + \gamma_u(i) \tag{42}$$

where x_u, h_u, v_u and γ_u are uniform random values. Considering the operating range of the missile and the general degree of error of the inertial navigation system, the ranges of x_u, h_u, v_u, and γ_u are constrained within $10\ m$, $10\ m$, $5\ m/s$, and $0.1\ deg$, respectively. Monte Carlo simulations are performed to verify the performance against uncertainty. Table IV shows the Monte Carlo simulation results under the influence of uncertainty.

TABLE IV: Velocity Error with Uncertainty.

Number of Simulations	Average	Standard Deviation
300	$3.42m/s$	8.17

According to the Monte Carlo simulation, the lowest terminal velocity error is $0.2m/s$ and the highest terminal velocity error is $14.7m/s$. The simulation results in Table IV show that the average velocity errors are within 1%.

It is confirmed that even if uncertainty enters randomly, a trajectory is generated in the direction of reducing the velocity error by generating an appropriate trajectory in real time. Figs. 11a) and 11b) show the three representative profiles of the trajectory and velocity responses.

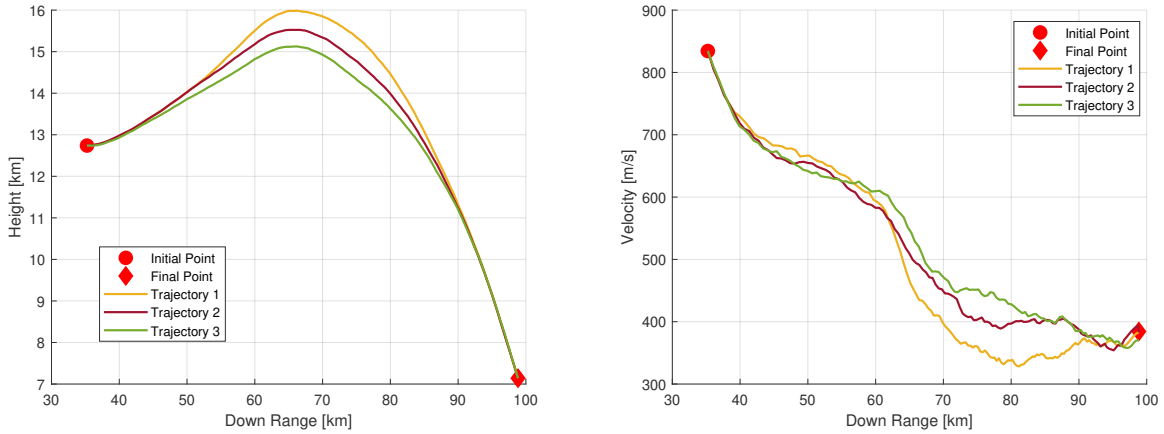

(a) Trajectory of the missile with uncertainty.

(b) Velocity of the missile with uncertainty.

Fig. 11: Simulation Results with Uncertainties

F. 6-DOF Simulation in Real Time

In the previous sections, numerical simulations were performed in a 3-DOF environment. Here, numerical simulations are performed in a 6-DOF environment to determine whether the proposed algorithm can be applied to the developed missiles. The 6-DOF simulation is constructed based on Fig. 1. The equations for the 6-DOF simulations are as follows:

$$X = m(\dot{u} + qw - rv) + mgsin\theta \tag{43}$$

$$Y = m(\dot{v} + ru - pw) - mgcos\theta sin\phi \tag{44}$$

$$Z = m(\dot{w} + pv - qu) - mgcos\theta cos\phi \tag{45}$$

$$L = I_{xx}\dot{p} - I_{xz}\dot{r} + qr(I_{zz} - I_{yy}) - I_{xz}pq \tag{46}$$

$$M = I_{yy}\dot{q} - rp(I_{xx} - I_{zz}) + I_{xz}(p^2 - r^2) \tag{47}$$

$$N = -I_{xz}\dot{p} + I_{zz}\dot{r} + pq(I_{yy} - I_{xx}) + I_{xz}qr \tag{48}$$

where p, q, r are angular rates, L, M, N are moments in roll, pitch, and yaw directions, respectively, u, v, w are each axis component of velocity, and X, Y, Z are force element on each body axis. I denotes the moment of inertia.

Table V summarizes the information of the initial and final points.

Aerodynamic coefficients C_L and C_D are defined as a function of velocity and angle-of-attack considering the shape of the missile. The proposed framework is applied after burnout with a true navigation model. It is assumed that the missile considered in this study is symmetrically equipped with four fins. In the 6-DOF simulation, the

TABLE V: Initial Point, Intermediate Point and Final Point

	Down Range	Cross Range	Height	Velocity	Flight Path Angle
Initial Point	$0.0\ km$	$0.5\ km$	$30.0\ km$	$850.0\ m/s$	$-30.0\ deg$
Final Point	$50.0\ km$	$0.05\ km$	$10.0\ km$	$400.0\ m/s$	$-40.0\ deg$

performance index explained in Sec. IV-A is used. Proportional navigation guidance law is used for horizontal plane guidance.

To demonstrate the performance of the proposed framework in various environments, simulations are performed for various cases. First, the results are analyzed compared to IAC, which is the optimal impact angle control. Second, the simulation results are compared by changing the final required velocity, which show that the proposed algorithm provides results satisfying various final conditions even under the same initial conditions. The final velocity modified for comparison is $350\ m/s$. Third, the results for 6-DOF system considering wind and without considering wind are compared. It is possible to study the robustness of the proposed framework with respect to the wind, which is one of representative disturbances. The wind with a maximum speed of $20m/s$ is considered. Finally, the effect on the drag is studied. Drag is a parameter that interferes with the analytical approach for the terminal velocity problem. Moreover, the drag coefficient is the most unpredictable parameter. By studying the effects of the drag, the limitation of the proposed framework can be investigated. In this simulation, the error for the drag is set as 5%.

Table VI summarizes various 6-DOF simulation results. In each simulation, the guidance command is fixed near the final point, $5sec$ before reaching the final point, to prevent the divergence of the guidance command. The results show that there exist small errors in altitude, h_{err}, and flight path angle, γ_{err}, in all simulations. IAC is a guidance law that reduces the terminal flight path angle error while flying to the final point, and the proposed framework considers a performance index to meet the terminal flight path angle. The performance of the proposed framework can be represented by the terminal velocity error, v_{err}, in Table VI. Simulations are constructed by C language on the same computer using previous simulations.

TABLE VI: 6-DOF Simulation Results

	h_{err}	V_{err}	γ_{err}
IAC	$-0.30\ km$	$-74.5\ m/s$	$0.34\ deg$
Replanning	$-0.17\ km$	$0.6\ m/s$	$0.91\ deg$
Replanning + $\lvert V_f\rvert = 350\ m/s$	$-0.18\ km$	$-5.4\ m/s$	$0.81\ deg$
Replanning + Wind	$-0.17\ km$	$-6.9\ m/s$	$0.89\ deg$
Replanning + Drag -5%	$-0.16\ km$	$-22.4\ m/s$	$0.96\ deg$
Replanning + Drag $+5\%$	$-0.17\ km$	$12.4\ m/s$	$0.91\ deg$

The terminal velocity error of the proposed framework is a very small compared to IAC. The missile using the proposed method flies by the generated trajectory, even if the terminal speed varies. Wind increases the terminal

velocity error because the wind continuously affects the missile until the missile reaches the target point. Drag force has more influence than other factors. As described in (26), the velocity is greatly affected by drag force. Therefore, if drag different from expected is continuously reflected, the terminal velocity error will inevitably increase. Assuming that the range of the terminal speed error is within 10% of the terminal speed, if the uncertainty of drag force is entered as -9%, the error range is exceeded. Even if an unexpected effects such as wind and drag are applied, the error is not large considering the velocity of the ballistic missile. Fig. 12 shows the results of 6-DOF simulation.

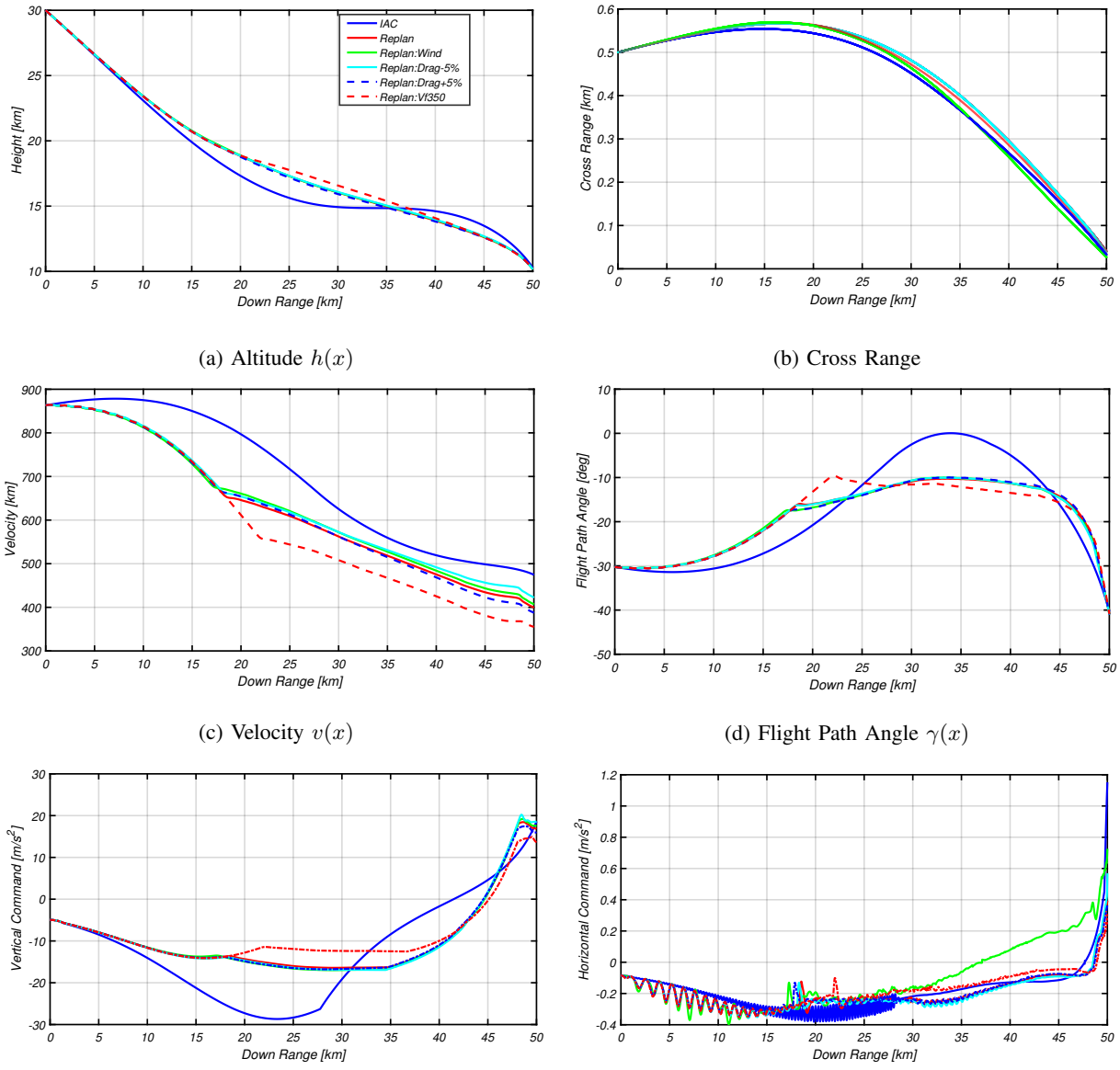

(a) Altitude $h(x)$

(b) Cross Range

(c) Velocity $v(x)$

(d) Flight Path Angle $\gamma(x)$

(e) Acceleration Command: Vertical

(f) Acceleration Command: Horizontal

Fig. 12: 6-DOF Simulation Results

While it is natural to satisfy the terminal velocity conditions, it can increase areas to be designed in the autopilot,

which can burden developers, and if they have to fly in limited areas for diplomatic and safety reasons, it can burden trajectory generation.

The computation time in a 6-DOF environment was calculated to determine whether or not it can be implemented in real-time. Because Δt directly affects the computation time, computation time is analyzed for various Δt. Initial and final points in Table V were used. For the proposed framework, the computation time is defined as the time including the process of generating the trajectory. And predicting the velocity error was measured. Simulations were performed by changing the parameter r 100 times to obtain the results in various environments. The average computation time of the 6-DOF simulation by varying Δt is summarized in Table VII.

TABLE VII: Average Computation Time of 6-DOF by varying Δt

Δt	$0.001\ sec$	$0.01\ sec$	$0.1\ sec$	$1.0\ sec$
Average Time	$0.266\ sec$	$0.042\ sec$	$< 0.001\ sec$	$< 0.001\ sec$

As described in Sec. V-C, the parameter Δt does not significantly affect the prediction terminal velocity. The computation time is less than $0.001\ sec$, which means that the proposed framework can be implemented and operated in the actual platform.

VI. Conclusions

Achieving a desired velocity at the final time is a challenging design problem in gliding vehicle guidance. The problem cannot be solved analytically because the nonlinearity and the model dependency of the velocity dynamics prohibit closed-form prediction. To address this problem, a trajectory planning framework was proposed for gliding missiles to achieve the desired terminal velocity considering the uncertainties in the environment. A quadratic programming formulation was adopted for trajectory generation. A family of trajectories can be generated depending on the objective function and constraints in the optimization problem. The trajectory equation was constructed to express the altitude as a function of the downrange to predict terminal velocity with a reduced number of equations instead of solving entire motion equations. The Euler method was utilized to predict the terminal velocity for each trajectory. Simulations were performed with various design parameters to validate the performance of the proposed framework. Simulation results showed that the proposed trajectory planning method provides appropriate trajectories satisfying the terminal velocity constraints.

Appendix

Matrix $\mathbf{D}$

Matrix $\mathbf{D}$ is the certain form deriving the derivative term of the trajectory, $h(x)$, as

$$\begin{aligned}\frac{dh(x)}{dx} &= na_n x^{n-1} + (n-1)a_{n-1}x^{n-2} + \cdots + 2a_2 x + a_1 \\ &= \begin{pmatrix} a_n & a_{n-1} & \cdots & a_0 \end{pmatrix} \begin{pmatrix} 0 & n & 0 & \cdots & 0 \\ 0 & 0 & (n-1) & \cdots & 0 \\ \vdots & \vdots & \vdots & \ddots & \vdots \\ 0 & 0 & 0 & \cdots & 1 \\ 0 & 0 & 0 & \cdots & 0 \end{pmatrix} \begin{pmatrix} x^n \\ x^{n-1} \\ \vdots \\ x^0 \end{pmatrix} \\ &\triangleq \underline{\mathbf{C}}^T \mathbf{D} \underline{\mathbf{\Phi}}(x)\end{aligned} \tag{A.1}$$

where

$$\mathbf{D} = \begin{pmatrix} 0 & n & 0 & \cdots & 0 \\ 0 & 0 & (n-1) & \cdots & 0 \\ \vdots & \vdots & \vdots & \ddots & \vdots \\ 0 & 0 & 0 & \cdots & 1 \\ 0 & 0 & 0 & \cdots & 0 \end{pmatrix} \tag{A.2}$$

Matrix $\mathbf{E}$

Matrix $\mathbf{E}$ is the certain form deriving the second derivative of the trajectory.

$$\begin{aligned}
\frac{d^2h(x)}{dx^2} &= n(n-1)a_n x^{n-2} + (n-1)(n-2)a_{n-1}x^{n-3} + \cdots + 2a_2 \\
&= \begin{pmatrix} a_n & a_{n-1} & \cdots & a_0 \end{pmatrix} \begin{pmatrix} 0 & 0 & n(n-1) & 0 & \cdots & 0 \\ 0 & 0 & 0 & (n-1)(n-2) & \cdots & 0 \\ \vdots & \vdots & \vdots & \vdots & \ddots & \vdots \\ 0 & 0 & 0 & 0 & \cdots & 2 \\ 0 & 0 & 0 & 0 & \cdots & 0 \\ 0 & 0 & 0 & 0 & \cdots & 0 \end{pmatrix} \begin{pmatrix} x^n \\ x^{n-1} \\ \vdots \\ x^0 \end{pmatrix} \\
&= \begin{pmatrix} a_n & a_{n-1} & \cdots & a_0 \end{pmatrix} \begin{pmatrix} 0 & n & 0 & \cdots & 0 \\ 0 & 0 & (n-1) & \cdots & 0 \\ \vdots & \vdots & \vdots & \ddots & \vdots \\ 0 & 0 & 0 & \cdots & 1 \\ 0 & 0 & 0 & \cdots & 0 \end{pmatrix} \begin{pmatrix} 0 & 0 & 0 & 0 & \cdots & 0 \\ 0 & 0 & (n-1) & 0 & \cdots & 0 \\ \vdots & \vdots & \vdots & \ddots & \vdots & \vdots \\ 0 & 0 & 0 & 0 & \cdots & 1 \\ 0 & 0 & 0 & 0 & \cdots & 0 \end{pmatrix} \begin{pmatrix} x^n \\ x^{n-1} \\ \vdots \\ x^0 \end{pmatrix} \\
&\triangleq \underline{\mathbf{C}}^T \mathbf{D}\mathbf{E}\underline{\mathbf{\Phi}}(x)
\end{aligned} \tag{A.3}$$

where

$$\mathbf{E} = \begin{pmatrix} 0 & 0 & 0 & 0 & \cdots & 0 \\ 0 & 0 & (n-1) & 0 & \cdots & 0 \\ \vdots & \vdots & \vdots & \ddots & \vdots & \vdots \\ 0 & 0 & 0 & 0 & \cdots & 1 \\ 0 & 0 & 0 & 0 & \cdots & 0 \end{pmatrix} \tag{A.4}$$

Matrix $\mathbf{F}$

Matrix $\mathbf{F}$ is the matrix form integrating the square of the second derivative of the trajectory.

$$
\begin{aligned}
&\int_{x_i}^{x_f} \left(\frac{d^2h(x)}{dx^2}\right)^2 dx \\
&= \int_{x_i}^{x_f} (\underline{\mathbf{C}}^T \mathbf{D}\mathbf{E}\underline{\mathbf{\Phi}}(x))^2 dx \\
&= \underline{\mathbf{C}}^T \mathbf{D}\mathbf{E} \int_{x_i}^{x_f} (\underline{\mathbf{\Phi}}(x)\underline{\mathbf{\Phi}}(x)^T) dx \mathbf{E}^T \mathbf{D}^T \underline{\mathbf{C}} \\
&= \underline{\mathbf{C}}^T \mathbf{D}\mathbf{E} \int_{x_i}^{x_f} \begin{pmatrix} x^{2n} & x^{2n-1} & \cdots & x^n \\ x^{2n-1} & x^{2n-2} & \cdots & x^{n-1} \\ \vdots & \vdots & \ddots & \vdots \\ x^n & x^{n-1} & \cdots & x^0 \end{pmatrix} dx \mathbf{E}^T \mathbf{D}^T \underline{\mathbf{C}} \\
&= \underline{\mathbf{C}}^T \mathbf{D}\mathbf{E} \begin{pmatrix} \frac{1}{2n+1}(x_f^{2n+1} - x_i^{2n+1}) & \frac{1}{2n}(x_f^{2n} - x_i^{2n}) & \cdots & \frac{1}{n+1}(x_f^{n+1} - x_i^{n+1}) \\ \frac{1}{2n}(x_f^{2n} - x_i^{2n}) & \frac{1}{2n-1}(x_f^{2n-1} - x_i^{2n-1}) & \cdots & \frac{1}{n}(x_f^n - x_i^n) \\ \vdots & \vdots & \ddots & \vdots \\ \frac{1}{n+1}(x_f^{n+1} - x_i^{n+1}) & \frac{1}{n}(x_f^n - x_i^n) & \cdots & x_f - x_i \end{pmatrix} \mathbf{E}^T \mathbf{D}^T \underline{\mathbf{C}} \\
&\triangleq \underline{\mathbf{C}}^T \mathbf{D}\mathbf{E}\mathbf{F}\mathbf{E}^T \mathbf{D}^T \underline{\mathbf{C}}
\end{aligned}
\tag{A.5}
$$

where

$$
\mathbf{F} = \begin{pmatrix} \frac{1}{2n+1}(x_f^{2n+1} - x_i^{2n+1}) & \frac{1}{2n}(x_f^{2n} - x_i^{2n}) & \cdots & \frac{1}{n+1}(x_f^{n+1} - x_i^{n+1}) \\ \frac{1}{2n}(x_f^{2n} - x_i^{2n}) & \frac{1}{2n-1}(x_f^{2n-1} - x_i^{2n-1}) & \cdots & \frac{1}{n}(x_f^n - x_i^n) \\ \vdots & \vdots & \ddots & \vdots \\ \frac{1}{n+1}(x_f^{n+1} - x_i^{n+1}) & \frac{1}{n}(x_f^n - x_i^n) & \cdots & x_f - x_i \end{pmatrix} \tag{A.6}
$$

Matrix $\mathbf{G}$

Matrix $\mathbf{G}$ is the matrix form integrating the trajectory.

$$
\begin{aligned}
\int_{x_i}^{x_f} h(x) dx &= \underline{\mathbf{C}}^T \int_{x_i}^{x_f} \underline{\mathbf{\Phi}}(x) dx \\
&= \underline{\mathbf{C}}^T \begin{pmatrix} \frac{1}{n+1}(x_f^{n+1} - x_i^{n+1}) \\ \frac{1}{n}(x_f^n - x_i^n) \\ \vdots \\ x_f - x_i \end{pmatrix} \\
&\triangleq \underline{\mathbf{C}}^T \mathbf{G}
\end{aligned}
\tag{A.7}
$$

where

$$\mathbf{G} = \begin{pmatrix} \dfrac{1}{n+1}(x_f^{n+1} - x_i^{n+1}) \\ \dfrac{1}{n}(x_f^{n} - x_i^{n}) \\ \vdots \\ x_f - x_i \end{pmatrix} \tag{A.8}$$

REFERENCES

[1] Y. Kim, N. Cho, J. Park, and Y. Kim, "Design framework for optimizing waypoints of vehicle trajectory considering terminal velocity and impact angle constraints," *Engineering Optimization*, Published Online, 2021.

[2] F. Perkins, *Derivation of Linear-Tangent Steering Laws*, Air Force Report No. SSD-TR-66-211. Air Force Systems Command, Los Angeles, CA, Nov. 1966.

[3] D. Chandler and I. Smith, "Development of the iterative guidance mode with its application to various vehicles and missions," *Journal of Spacecraft and Rockets*, vol. 4, no. 7, pp. 898–903, 1967.

[4] R. Jaggers, "An explicit solution to the exoatmospheric powered flight guidance and trajectory optimization problem for rocket propelled vehicles," *AIAA Guidance and Control Conference*, Hollywood, FL, Aug. 1977.

[5] R. McHenry, A. Long, B. Cockrell, J. Thibodeau, III, and T. Brand, "Space shuttle ascent guidance, navigation, and control," *Journal of the Astronautical Sciences*, vol. 27, no. 1, pp. 1–38, 1979.

[6] S. Sinha and S. Shrivastava, "Optimal explicit guidance of multistage launch vehicle along three-dimensional trajectory," *Journal of Guidance, Control, and Dynamics*, vol. 13, no. 3, pp. 394–403, 1990.

[7] W. Williamson, R. Greene, and D. Hull, "Application of the perturbation method to optimal shuttle reentry trajectories," *Engineering Optimization*, vol. 2, no. 3, pp. 189–196, 1976.

[8] P. Zarchan, *Tactical and Strategic Missile Guidance*, 3rd Ed., Progress in Astronautics and Aeronautics. AIAA, Washington, DC, 1990.

[9] J. White, "Guidance and targeting for the strategic target system," *Journal of Guidance, Control, and Dynamics*, vol. 15, no. 6, pp. 1313–1319, 1992.

[10] J. White, "Cut-off insensitive guidance with variable time of flight," *AIAA Guidance and Control Conference*, Monterey, CA, Aug. 1993.

[11] S. Kim and T. Um, "Flight-path angle control for cutoff insensitive guidance," *Journal of Guidance, Control, and Dynamics*, vol. 38, no. 4, pp. 706–710, 2015.

[12] S. Wang, F. Liu, T. Chao, and M. Yang, "Robust spline-line energy management guidance algorithm with multiple constraints and uncertainties for solid rocket ascending," *Chinese Journal of Aeronautics*, vol. 35, no. 2, pp. 214–234, 2022.

[13] J. Roshanian, A. A. Bataleblu, and M. Ebrahimi, "Robust ascent trajectory design and optimization of a typical launch vehicle," *Journal of Mechanical Engineering Science*, vol. 232, no. 24, pp. 4601–4614, 2018.

[14] C. Dong and Y. Cai, "Reentry trajectory optimization for hypersonic glide vehicle with flexible initial conditions," *Journal of Aerospace Engineering*, vol. 30, no. 5, 2017.

[15] G. Sushnigdha and A. Joshi, "Reentry trajectory design with pigeon inspired optimization using derived angle of attack profile," *Journal of Aerospace Engineering*, vol. 31, no. 6, 2018.

[16] J. Kraemer and H. Ehlers, "Shuttle orbiter guidance system for the terminal flight phase," *IFAC Proceedings Volumes*, vol. 8, Issue 1, Part 4, pp. 328–337, 1975.

[17] R. Wang, S. Tang, and D. Zhang, "Short-range reentry guidance with impact angle and impact velocity constraints for hypersonic gliding reentry vehicle," *IEEE Access*, vol. 7, pp. 47 437–47 450, 2019.

[18] X. Lan, W. Xu, and Y. Wang, "3d profile reconstruction and guidance for the terminal area energy management phase of an unpowered rlv with aerosurface failure," *Journal of Aerospace Engineering*, vol. 33, no. 3, p. 04020003, 2020.

[19] P. C. Eng, "Path planning, guidance and control for a uav forced landing," Ph.D. dissertation, School of Engineering Systems, Queensland University of Technology, Brisbane, QLD, Australia, 2011.

[20] R. T. Farouki, "Construction of g1 planar hermite interpolants with prescribed arc lengths," *Computer Aided Geometric Design*, vol. 46, pp. 64–75, 2016.

[21] C. Sánchez-Sánchez and D. Izzo, "Real-time optimal control via deep neural networks: Study on landing problems," *Journal of Guidance, Control, and Dynamics*, vol. 41, no. 5, pp. 1122–1135, 2018.

[22] Y.-S. Kim and M.-J. Tahk, "Auto-landing guidance for unmanned aerial vehicle with engine flame-out," *Proceedings of the Institution of Mechanical Engineers, Part G: Journal of Aerospace Engineering*, vol. 233, no. 13, pp. 4864–4878, 2019.

[23] Y. Shi and Z. Wang, "Computational missile guidance: A deep reinforcement learning approach," *Journal of Aerospace Information Systems*, vol. 18, no. 8, pp. 571–582, 2021.

[24] J. Kim, S. Lee, S. Lee, Y. Kim, and C. Song, "Neural-network-based path replanning for gliding vehicles considering terminal velocity," *IEEE Access*, vol. 9, pp. 78 701–78 714, 2021.

[25] S. He, H.-S. Shin, and A. Tsourdos, "Onboard generation of optimal trajectories for hypersonic vehicles using deep learning," *Journal of Spacecraft and Rockets*, vol. 58, no. 2, pp. 400–414, 2021.

[26] V. M. Goncalves, L. C. A. Pimenta, C. A. Maia, B. C. O. Dutra, and G. A. S. Pereira, "Vector fields for robot navigation along time-varying curves in n-dimensions," *IEEE Transactions on Robotics*, vol. 26, no. 4, pp. 647–659, 2010.

[27] Y. Liang and Y. Jia, "Tangent vector field approach for curved path following with input saturation," *Systems and Control Letters*, vol. 104, pp. 49–58, 2017.

[28] S. Lee, Y. Kim, and C. Song, "Impact angle control guidance of glide-capable munition using a vector field approach," *IEEE Transactions on Aerospace and Electronic Systems*, vol. 57, no. 2, pp. 1069–1083, 2021.

[29] W. Li, Y. Zhu, and D. Zhao, "Missile guidance with assisted deep reinforcement learning for head-on interception of maneuvering target," *Complex and Intelligent Systems*, vol. 7, pp. 1–12, 2021.

[30] J. Patha and R. McGehee, "Guidance, energy management, and control of a fixed-impulse solid-rocket vehicle during orbit transfer," *AIAA Guidance and Control Conference*, San Diego, CA, Aug. 1976.

[31] T. Kuroda and F. Imado, "A mid-course guidance law for highly maneuverable thrust vector control missiles," *AIAA Guidance, Navigation, and Control Conference*, New Orleans, LA, Aug. 1997.

[32] H. Xu and W. Chen, "An energy management ascent guidance algorithm for solid rocket-powered launch vehicles," *17th AIAA International Space Planes and Hypersonic Systems and Technologies Conference*, San Francisco, CA, Apr. 2011.

[33] H. Zhou, T. Rahman, and W. Chen, "Impact angle and impact velocity constrained terminal guidance for stationary target," *Aircraft Engineering and Aerospace Technology*, vol. 87, pp. 454–464, 2015.

[34] S.-Y. Chen and Q.-L. Xia, "A multiconstrained ascent guidance method for solid rocket-powered launch vehicles," *International Journal of Aerospace Engineering*, vol. 2016, Article ID 6346742, 2016.

[35] M. Tahk, G. Moon, and S. Shim, "Augmented polynomial guidance with terminal speed constraints for unpowered aerial vehicles," *International Journal of Aeronautical and Space Sciences*, vol. 20, no. 1, pp. 183–194, 2019.

Online trajectory replan for gliding vehicle considering terminal velocity constraint

Kim, Youngil

2022-08-08

Kim Y, Cho N, Park J, Kim Y. (2023) Online trajectory replan for gliding vehicle considering terminal velocity constraint. IEEE Transactions on Aerospace and Electronic Systems, Volume 59, Issue 2, April 2023, pp. 1067-1083

https://doi.org/10.1109/TAES.2022.3197103